Spin, charge, and orbital ordering in $R\mathrm{BaMn_2O_{5+\delta}}$ (R=Y, La; $0 \leqslant \delta \leqslant 1$) and their dependence on oxygen content and size of the R constituent

R. Vidya,* P. Ravindran, A. Kjekshus, and H. Fjellvåg
Center for Materials Science and Nanotechnology, Department of Chemistry, University of Oslo, Box 1033 Blindern, N-0315 Oslo, Norway

(Received 11 September 2006; revised manuscript received 17 April 2007; published 16 November 2007)

The effect of oxygen content on spin, charge, and orbital ordering in $R\mathrm{BaMn_2O_{5+\delta}}$ (R=Y, La; $0 \leqslant \delta \leqslant 1$) is studied by density-functional-theory-based calculations as implemented in the full-potential linearized-augmented plane-wave method. Structural optimizations using the projector augmented wave method have been performed for all the phases and the calculated structural parameters are found to be in good agreement with experimental values. Total-energy calculations have systematically been performed including force as well as stress minimization for paramagnetic, ferromagnetic, and antiferromagnetic configurations. For $\delta=0$, the ground state is found to be ferrimagnetic, whereas the variants with oxygen contents $\delta=1/2$ and 1 give rise to an antiferromagnetic ground state, all in perfect agreement with experimental findings. The electronic-band characteristics are analyzed using total and site- and orbital-projected densities of states and the examination shows that the electronic structure undergoes a gradual change from semiconductor-to-metal behavior on going from $\delta=0$ to 1. Even the GGA+U approach failed to reproduce the insulating state for the phases with $\delta=1$, indicating that introduction of the experimental *CE*-type magnetic structure may be important. The charge and orbital ordering are analyzed with the help of the energy-projected-density matrices of the d electrons. Very different ordering patterns have emerged for the different phases under investigation, indicating that both cation radii and oxygen stoichiometry play an important role in deciding spin, charge, and orbital ordering.

DOI: 10.1103/PhysRevB.76.195114 PACS number(s): 71.20.−b, 81.05.Je, 71.15.Nc

I. INTRODUCTION

Double perovskite variants with the general formula $R_{1-x}A_x\mathrm{Mn_2O_{5+\delta}}$ ($0 \leqslant x \leqslant 1$; R=rare-earth element, A=alkaline-earth element; $0 \leqslant \delta \leqslant 1$) have been extensively investigated over the last decade. Potential technological applications have greatly stimulated the research activity and the scientific community has benefited from these efforts in the form of improved comprehension of these systems. Many interesting features such as colossal magnetoresistance, metal-insulator transitions, and spin, charge, and orbital ordering (SO, CO, and OO) are certainly associated with each other in this special class of materials. Such enchanting phenomena are believed to be caused by competition between the spin, charge, and orbital degrees of freedom.

In general, there will be disorder in the lattice when A and R in the proportion x to $(1-x)$ are randomly distributed in the appropriate sublattices of the structure. However, for $x=1/2$, proper cation-ordered double perovskites ($RA\mathrm{Mn_2O_6}$) are formed with alternate stacking of layers of R and A along the c axis (the orientation of the unit cell requires in some cases space group transformation). Structural and physical properties of such a structural arrangement have been recently reported[1] for R=Y and La to Er. Owing to the cation-size mismatch and Jahn-Teller distortion (JTD), the $RA\mathrm{Mn_2O_6}$ phases undergo transition between paramagnetic-metal and antiferromagnetic-insulator states and CO transitions occur at relatively high temperatures. An interesting aspect of the $RA\mathrm{Mn_2O_6}$ phases with R=Y and La is their ability to form stable oxygen-deficient variants, here more conveniently represented by the reverse formula $RA\mathrm{Mn_2O_{5+\delta}}$ and conceptually added oxygen. The oxygen deficiencies are normally formed in the R layers of such structures.

One of the parameters used to describe CO is the transfer integral t between Mn d and O p states. When the t value is high, electrons are imagined to be able to hop from one Mn atom to another via an appropriately arranged intervening O atom, giving rise to metal-like couplings between electrons known as the double-exchange interaction. However, when t is small, the electrons get localized on the Mn sites and this ultimately results in CO. Thus, the oxygen content and population of the oxygen orbitals relative to the Mn d orbitals govern the metal-insulator transitions and play an important role in the SO, CO, and OO mechanisms. We have earlier reported on the influence of the oxygen occupancy on the CO and OO in $\mathrm{LaBaMn_2O_{5+\delta}}$,[2] and, in this report, we give an account for our findings for $\mathrm{YBaMn_2O_{5+\delta}}$. The aim has been to evaluate the composite effects of oxygen content and size mismatch of the constituents of $RA\mathrm{Mn_2O_{5+\delta}}$ on CO and OO phenomena. In systems with R=Y, La to Er and A=Ba, the mismatch between the RO and BaO layers is smallest for the La-Ba combination and largest for Y-Ba. Hence, systems comprising Y and La constituents should be good candidates to analyze the effect of R atomic size on CO and OO phenomena.

The composition of the present phases is chosen so that for $\delta=0$, the equal amounts of Y or La and Ba lead to equal amounts of Mn atoms in the formal ionic valence states 2+ and 3+, thus maximizing the Coulomb stabilization energy of the CO state. In the same breath, phases with $\delta=1/2$ should exhibit only Mn^{3+} and those with $\delta=1$ should have the formal ionic states Mn^{3+} and Mn^{4+}. In fact, experimental[3,4] and theoretical studies[2,5] have confirmed that $\mathrm{YBaMn_2O_5}$ and $\mathrm{LaBaMn_2O_5}$ carry two different types of Mn atoms with simultaneous CO, OO, and ferrimagnetic (ferri) SO. Since we have earlier analyzed the magnetic and elec-

tronic properties of $YBaMn_2O_5$ (Ref. 5) and $LaBaMn_2O_5$ (Ref. 2) in detail, an obvious challenge is to perform a comparative analysis of the two $RAMn_2O_{5+\delta}$ systems.

II. COMPUTATIONAL DETAILS

In the present calculations, we have made use of the density-functional-theory (DFT) approach implemented in the full-potential linearized-augmented plane-wave (FPLAPW-WIEN2K) method[6] in a fully relativistic version (including spin-orbit coupling). The charge densities and potentials in the atomic spheres were represented by spherical harmonics up to $\ell=6$, whereas in the interstitial region, these quantities were expanded in Fourier series. Atomic-sphere radii R_{MT} of 2.2, 2.3, 1.9, and 1.6 a.u. for Y, La, Ba, Mn, and O, respectively, were used. We earlier noted that the resulting magnetic moments do not depend appreciably on the chosen atomic-sphere radii. We used the $R_{mt}\star K_{max}$ value of 7 and $G_{max}=12$. The initial basis set included 5*s*, 5*p*, and 4*d* valence and 4*s* and 4*p* semicore functions for Y, 6*s*, 6*p*, and 6*d* valence and 5*s* and 5*p* semicore functions for La and Ba, 4*s*, 4*p*, and 3*d* valence and 3*s* and 3*p* semicore functions for Mn, and 2*s*, 2*p*, and 3*d* functions for O. The Brillouin zone (BZ) integration was done with a modified tetrahedron method[7] using approximately 200 **k** points in the irreducible wedge of BZ, depending on the crystal structure of the phase in question. Exchange and correlation effects are treated under the generalized-gradient approximation (GGA)[8] including the Perdew-Burke-Ernzerhof functional. In an effort to account for the strong correlation effects, we have also performed GGA+*U* calculations for all phases subject to this study. These calculations are based on a method introduced by Anisimov *et al.*[9] as implemented in the WIEN2K package.[10] Based on our previous experience on transition-metal oxides, we used empirical parameters of $U=4.0$ eV and $J=0.95$ eV in the GGA+*U* calculations.

In order to visualize OO patterns, we have made use of the energy-projected occupation-density matrices for the *d* orbitals of Mn atoms in the studied systems. The present method has the additional advantage that the orientation and magnitude of filling of a particular orbital can be correctly deduced.

The structural optimization calculations have been performed using the projected augmented plane-wave[7] method as implemented in the Vienna *ab initio* simulation package (VASP).[11] The optimization of the atomic geometry was performed via a conjugate-gradient minimization of the total energy, using Hellmann-Feynman forces on the atoms and the stresses in the unit cell. During the simulations, atomic coordinates and axial ratios were allowed to relax for different volumes of the unit cell. Convergence minimum with respect to atomic relaxations was assumed to have been attained when the energy difference between two successive iterations was less than 10^{-6} eV per unit cell and the forces acting on the atoms were less than 1 meV $Å^{-1}$. A plane-wave energy cutoff of 700 eV was used in all calculations.

III. RESULTS AND DISCUSSION

A. Crystal structures

1. $R\mathrm{BaMn_2O_5}$

The optimized structural parameters for $R\mathrm{BaMn_2O_{5+\delta}}$ are given in Table I and are found to be in good agreement with experimental values. The optimized unit-cell volumes are somewhat overestimated by 1%–2% but well within the 3% limit accepted for calculations based on DFT and GGA. $YBaMn_2O_5$ and $LaBaMn_2O_5$ crystallize in the tetragonal $YBaCuFeO_5$-type structure (Refs. 3 and 4, space group $P4/nmm$). Reader may refer Sec. III D for crystal structure figures. Oxygen-vacant Y or La and oxygen-full Ba layers are formed alternatively along the *c* axis. Two crystallographically different Mn atoms are situated in square-pyramidal coordination with their oxygen neighbors. Associated with the different sizes of Y and Ba, the corresponding Mn-O bond lengths as well as Mn-O-Mn bond angles become appreciably different and these features are known to play crucial roles in the physical properties of these materials.

2. $R\mathrm{BaMn_2O_{5.5}}$

The $YBaMn_2O_{5.5}$ and $LaBaMn_2O_{5.5}$ phases ascribe an orthorhombic structure (Refs. 4 and 12, space group *Ammm*). The extra oxygen atoms compared with the $\delta=0$ cases partially occupy the earlier oxygen-empty Y or La layers. Therefore, half of the square pyramids gain an extra oxygen atom and change their coordination polyhedra from square pyramids to octahedra.

3. $R\mathrm{BaMn_2O_6}$

In $YBaMn_2O_6$ and $LaBaMn_2O_6$, the oxygen content of the originally oxygen-empty Y or La layers at $\delta=0$ has become completely filled up and all the earlier square pyramids are converted into octahedra. A notable distinction between $YBaMn_2O_6$ and $LaBaMn_2O_6$ is that the former takes a low-symmetric monoclinic structure (space group *P*2, also reported to be triclinic[13]), whereas the latter adopts a tetragonal structure (Ref. 4, space group $P4/mmm$). The influence of the size mismatch between the constituents is best seen for $\delta=1$, where the Y-based phase exhibits highly distorted octahedra, whereas those of the La variant are more regular. $YBaMn_2O_6$ contains two crystallographically nonequivalent Mn sites (Mn1 and Mn2) and eight crystallographically different oxygen sites. The two kinds of MnO_6 octahedra in $YBaMn_2O_6$ show large variation in Mn-O-Mn bond angles (157.5° to 176.8°) and a remarkable difference even in the average Mn-O distances (1.96 Å for Mn1-O and 1.93 Å for Mn2-O). The nature and magnitude of the octahedral tilting depend not only on the Y-to-Ba vs La-to-Ba mismatch but also on the coordination preference for Y and La, covalence effects, JTD, etc. Using the Goldschmidt tolerance factor as an indicator, the MnO_2 layer in $YBaMn_2O_6$ should feel opposite oriented strain forces (viz., be subjected to structural frustration) from the adjacent Y-O and Ba-O layers. Because of this frustration, the structural mismatch cannot be compensated by mere tilting of the MnO_6 octahedra. As a con-

TABLE I. Optimized ground-state structural parameters for $R\mathrm{BaMn_2O_{5+\delta}}$. Experimental values are given in the parentheses.

Phase	Unit cell (Å or Å^3)	Atom	Site	x	y	z
$YBaMn_2O_5$	a=5.5643 (5.5359)	Y	2b	1/4 (1/4)	3/4 (3/4)	1/2 (1/2)
Expt. (Ref. 12)	c=7.6176 (7.6151)	Ba	2a	1/4 (1/4)	3/4 (3/4)	0 (0)
	V=235.85 (233.37)	Mn1	2c	1/4 (1/4)	1/4 (1/4)	0.2760 (0.2794)
	Space group=$P4/nmm$	Mn2	2c	1/4 (1/4)	1/4 (1/4)	0.2582 (0.2514)
		O1	8j	0.4919 (0.4911)	0.4919 (0.4911)	0.3133 (0.3164)
		O2	2c	1/4 (1/4)	1/4 (1/4)	0.0019 (0.0061)
$LaBaMn_2O_5$	a=5.6525 (5.6386)	La	2b	1/4 (1/4)	3/4 (3/4)	1/2 (1/2)
Expt. (Ref. 14)	c=7.7760 (7.7799)	Ba	2a	1/4 (1/4)	3/4 (3/4)	0 (0)
	V=248.45 (247.35)	Mn1	2c	1/4 (1/4)	1/4 (1/4)	0.2647 (0.2637)
	Space group=$P4/nmm$	Mn2	2c	1/4 (1/4)	1/4 (1/4)	0.2496 (0.2489)
		O1	8j	0.4907 (0.4908)	0.4907 (0.4908)	0.7000 (0.7001)
		O2	2c	1/4 (1/4)	1/4 (1/4)	0.0020 (0.0061)
$YBaMn_2O_{5.5}$	a=3.8482 (3.7710)	Y	4j	1/2 (1/2)	0.2282 (0.2731)	0 (0)
Expt. (Ref. 1)	b=7.9903 (8.1590)	Ba	4f	1/2 (1/2)	1/4 (1/4)	1/4 (1/4)
	c=15.4809 (15.2709)	Mn1	4k	0 (0)	1/2 (1/2)	0.1159 (0.1145)
	V=476.01 (469.95)	Mn2	4k	0 (0)	1/2 (1/2)	0.3763 (0.3784)
	Space group=$Ammm$	O1	8h	0 (0)	0.2645 (0.2228)	0.0990 (0.1009)
		O2	4k	0 (0)	1/2 (0)	0.2518 (0.2525)
		O3	4j	1/2 (1/2)	0 (0)	0.0905 (0.0877)
		O4	4j	1/2 (1/2)	0 (0)	0.3880 (0.3843)
		O5	2c	0 (0)	1/2 (1/2)	1/2 1/2
$LaBaMn_2O_{5.5}$	a=3.8562 (3.8445)	La	4j	1/2 (1/2)	0.7648 (0.7327)	0 (0)
Expt. (Ref. 13)	b=8.2901 (8.1849)	Ba	4f	1/2 (1/2)	1/4 (1/4)	1/4 (1/4)
	c=15.6209 (15.4258)	Mn1	4g	0 (0)	1/2 (0)	0.8792 (0.8818)
	V=499.37 (485.40)	Mn2	4g	0 (0)	1/2 (0)	0.6252 (0.6263)
	Space group=$Ammm$	O1	8p	0 (0)	0.7279 (0.7688)	0.8968 (0.8923)
		O2	4g	0 (0)	1/2 (0)	0.2543 (0.2516)
		O3	4h	1/2 (1/2)	0 (0)	0.0987 (0.0960)
		O4	4h	1/2 (1/2)	0 (0)	0.3833 (0.3827)
		O5	2b	1/2 (1/2)	0 (0)	0 (0)
$YBaMn_2O_6$	a=5.5536 (5.5193)	Y	2a	0 (0)	0.7619 (0.7425)	0 (0)
Expt. (Ref. 1)	b=5.5242 (5.5131)	Ba	2a	1/2 (1/2)	0.7538 (0.7635)	0 (0)
	c=7.6487 (7.6135)	Mn1	2a	0.2433 (0.2430)	0.7498 (0.7565)	1/2 (1/2)
	β=90.58° (90.30°)	Mn2	2a	0.7567 (0.7570)	0.7498 (0.7565)	1/2 (1/2)
	V=234.64 (231.67)	O1	2a	0 (0)	0.8123 (0.7960)	1/2 (1/2)
	Space group=Pc	O2	2a	0.2006 (0.2035)	0.5197 (0.5015)	0.7711 (0.7720)
		O3	2a	0.7994 (0.7965)	0.5196 (0.5015)	0.2290 (0.2280)
		O4	2a	0.2421 (0.2420)	0.0220 (0.0135)	0.7298 (0.7280)
		O5	2a	0.7579 (0.7580)	0.0220 (0.0135)	0.2702 (0.2720)
		O6	2a	1/2 (1/2)	0.7259 (0.7215)	1/2 (1/2)
$YBaMn_2O_6$	a=5.4592 (5.5197)	Y	2i	0.7337 (0.7546)	0.2339 (0.2455)	0.5050 (0.5061)
Expt. (Ref. 13)	b=5.4591 (5.5138)	Ba	2i	0.7484 (0.7557)	0.2484 (0.2439)	0.9955 (0.9914)
	c=7.8811 (7.6032)	Mn1	2i	0.2501(0.2430)	0.2516 (0.2465)	0.2581 (0.2579)
	α=89.61° (90.02°)	Mn2	2i	0.2484 (0.2518)	0.2498 (0.2617)	0.7419 (0.7472)

TABLE I. (*Continued.*)

Phase	Unit cell (Å or Å^3)	Atom	Site	x	y	z
	β=90.41° (90.28°)	O1(a)	2*i*	0.4675 (0.4828)	0.4716 (0.5012)	0.2829 (0.2950)
	γ=90.85° (90.11°)	O1(b)	2*i*	0.5310 (0.5195)	0.0311 (0.0147)	0.2467 (0.2529)
	V=234.84 (231.40)	O2	2*i*	0.2979 (0.2556)	0.2021 (0.2776)	0.4999 (0.4953)
	Space group=$P\bar{1}$	O3	2*i*	0.2359 (0.1981)	0.2640 (0.2026)	0.5017 (0.5042)
		O4(a)	2*i*	0.0284 (0.0222)	0.9674 (0.9652)	0.2828 (0.2649)
		O4(b)	2*i*	0.9676 (0.9686)	0.5324 (0.5119)	0.3005 (0.2940)
$LaBaMn_2O_6$	a=3.9664 (3.9018)	La	1*b*	0 (0)	0 (0)	1/2 (1/2)
Expt. (Ref. 4)	c=7.7013 (7.7919)	Ba	1*a*	0 (0)	0 (0)	0 (0)
	V=121.16 (118.62)	Mn	2*h*	1/2 (1/2)	1/2 (1/2)	0.2522 (0.2528)
	Space group=$P4/mmm$	O1	4*i*	0 (0)	1/2 (1/2)	0.2698 (0.2655)
		O2	1*c*	1/2 (1/2)	1/2 (1/2)	0 (0)
		O3	1*d*	1/2 (1/2)	1/2 (1/2)	1/2 (1/2)

sequence, the shape of the octahedra becomes heavily deformed.[1] Moreover, the MnO_2 planar oxygen configuration is displaced toward the Y layer and away from Ba layer, resulting in shifts of the Mn and O atoms from the positions ascribed for ideal octahedral geometry. Even though the deviation from regular octahedral arrangement also has been observed in the structure of $LaBaMn_2O_6$, this phase only exhibits one crystallographically equivalent Mn site and the octahedra are only slightly distorted. Note that zero tilting of the coordination polyhedra is obtained only when there are vacant oxygen sites in the Y or La layers of $YBaMn_2O_5$ or $LaBaMn_2O_5$.

Since the experimental studies on $YBaMn_2O_6$ have reported two different structural arrangements at high temperatures [monoclinic $P2$ at 350 K (Ref. 1) and triclinic $P\bar{1}$ at 300 K (Ref. 13)], we have performed structural optimization for both structures in antiferromagnetic (AF) configuration. Large forces ($\sim$3.2 eV Å^{-1}) were found on the Mn sites in the input experimental $P2$ structure, so we performed a complete structural optimization, in which the stress and forces were minimized simultaneously, also taking into account the proper magnetic structures. Similarly in the triclinic structure, forces ranging from 0.6 to 1.2 eV Å^{-1} were found on the constituents at the start of the calculations. These calculations converged to the structure of the monoclinic variant, which was lower in energy by nearly 0.77 eV f.u.$^{-1}$ than the triclinic variant. Moreover, the total-energy gain on going from the experimental $P2$ to the optimized monoclinic structure amounted to nearly 1.01 eV f.u.$^{-1}$. However, the difference between the optimized and experimental unit-cell volumes is $\sim$1.64%, well within the limit accepted for DFT calculations. On analyzing the symmetry of the optimized monoclinic variant, we found that the structural parameters are in good agreement with the experimental determination,[1] but the atomic arrangements are slightly different obeying the space group Pc rather than the initial $P2$. It is worthy to note that the optimized structural parameters obtained from the present type of calculations are valid only for low temperatures. However, at high temperatures, the vibrational entropy contributes to the structural phase stability, which is not included in the present calculations. Nakajima *et al.*[1] have mentioned that the low temperature phase might have a monoclinic symmetry with possible space group $P2$, Pm, or $P2/m$. It can be seen that our structural optimization which is valid for low temperature (0 K) leads to a ground-state structure with space group Pc that is closely related to Pm. The optimized unit-cell dimensions and positional parameters for this (Pc) and triclinic description for the $YBaMn_2O_6$ structure are given in Table I. We believe that the vibrational entropy and/or deviation in the oxygen stoichiometry may be responsible for the stabilization of triclinic structure over the monoclinic structure experimentally established at finite temperatures. Moreover, if one takes the structural parameters for the $P2$-based structure and search for higher symmetric structure within a tolerance limit of 0.001 Å, then one would arrive at the theoretically identified Pc structure. (Note that in order to enable a direct comparison with the optimized parameters, experimental data are also described in space group Pc in Table I.) As $YBaMn_2O_6$ is believed to be strongly correlated, structural optimization has also been performed including GGA+U for both monoclinic and triclinic variants. After minimizing stress as well as forces acting on both variants by including U=4.0 eV and J=0.95 eV, the monoclinic structure with space group Pc is found to be lower in energy by 349 meV f.u.$^{-1}$ than the triclinic variant. We have used the optimized structural parameters in Table I to analyze magnetic and electronic properties of $YBaMn_2O_6$.

Owing to the different space and valence requirements for the Y and Ba atoms, the Mn1-O and Mn2-O bond lengths and the Mn1-O-Mn2 bond angles differ considerably and these distinctions are reflected in the physical properties of the $RBaMn_2O_{5+\delta}$ phases. Table II displays relevant bond lengths and bond angles according to the experimental structure determinations. The distances between the Mn and O_b (O atoms in the base plane of the coordination polyhedron, viz., plane parallel to the crystallographic ab plane) are

TABLE II. Bond lengths (in Å) and bond angles (in deg) between Mn and O in the experimentally determined structures of $R\mathrm{BaMn_2O_{5+\delta}}$ (δ=0, 1/2, and 1).

Specification	Y; δ=0	La; δ=0	Y; δ=1/2	La; δ=1/2	Y; δ=1	La; δ=1
R-O	2.406	2.530	2.568	2.642	2.773	2.716
Ba-O	2.937	2.945	2.962	2.938	2.774	2.759
Mn1-O1[a]	1.908	1.941	1.830; 1.929	1.893; 1.963	1.850; 1.810; 1.980	1.953
Mn1-O2[b]	2.081	2.004	2.107	2.025	2.080; 2.030; 2.050	1.970; 1.926
Mn2-O1	2.086	2.105	2.284; 1.888	2.231; 1.932	1.880; 1.800; 1.900; 1.990	
Mn2-O2	1.961	1.985	1.923; 1.857	1.898; 1.942	2.090; 1.950	
Mn1-O1-Mn2	157.8	160.8	165.53; 155.24	167.68; 168.82	172.4; 165.6; 157.5; 176.8; 162.9	174.19
Mn1-O2-Mn2	180	180	180; 174.53	180; 175.46	161.8; 172.3	180

[a]O in the base plane of the polyhedron.
[b]O at the apex of the polyhedron.

shorter in the Y phases than those in the corresponding La variants. The opposite is true for the distances between Mn and the apical oxygen atoms. The Mn1-Ob-Mn2 bond angles deviate much from 180°. The bond angles running along the apices of the polyhedra (oriented along *c* direction) is equal to, or deviate only little from, 180°. The deviation in bond angles from the ideal 180° is generally larger for *R*=Y than for La, which in itself is a hint of an effect of the size difference between Y and La. Among the considered phases, $\mathrm{YBaMn_2O_6}$ displays the overall largest distortion of the coordination polyhedra. The accumulated knowledge on the $R\mathrm{BaMn_2O_{5+\delta}}$ phases indicates that such materials may hide a lot of yet unexplored exotic physical properties. Therefore, it may be worthwhile to analyze more systematically their relevant physical properties in terms of the oxygen content and the size of the *R* and *A* constituents.

B. Magnetic properties: Spin ordering

1. $R\mathrm{BaMn_2O_5}$

We have performed a complete structural optimization for $R\mathrm{BaMn_2O_5}$ in paramagnetic (P), ferromagnetic (F), and different AF configurations; as seen from Table III, the AF state is preferred for all these phases. If one considers *A*-AF- and *G*-AF-type magnetic arrangements among the different AF configurations for $\mathrm{YBaMn_2O_5}$, the *A*-AF-type arrangement is higher in energy by 125 meV f.u.$^{-1}$ than the *G*-AF-type arrangement; for $\mathrm{LaBaMn_2O_5}$, it exceeds the *A*-AF type by 220 meV f.u.$^{-1}$. This implies that the *G*-AF-type arrangement is the ground state for both the phases. The calculated magnetic moments in the ground-state configuration are given in Table IV and are seen to be in good agreement with the available experimental data. Moreover, these phases have nonzero total moments and accordingly take a ferri ground state, in perfect agreement with experimental findings.[3,4] It should be noted that the magnetic moments at the Mn sites calculated by the GGA+*U* method are slightly higher than those calculated by the GGA method for $\mathrm{YBaMn_2O_5}$.

2. $R\mathrm{BaMn_2O_{5.5}}$

An explicit magnetic structure for $\mathrm{YBaMn_2O_{5.5}}$ is hitherto not reported, but $\mathrm{LaBaMn_2O_{5.5}}$ is reported[14] to take a magnetic structure with ferromagnetic spin ladders (SL) along the *b* axis that are AF coupled along the *a* and *c* axes. In order to establish the correct magnetic structure for $\mathrm{YBaMn_2O_{5.5}}$ and confirm the experimentally deduced magnetic structure of $\mathrm{LaBaMn_2O_{5.5}}$, we have performed a complete structural optimization for these phases in various magnetic configurations (see Fig. 1). The intraplane F interaction and interplane AF interaction give rise to the *A*-AF-type arrangement, whereas an intraplane AF and interplane F interactions result in *C*-AF-type arrangement. On the other hand, the intraplane as well as interplane AF interactions lead to the *G*-AF-type arrangement. In the experimentally deduced magnetic structure, each spin ladder lies along the *b* axis and is AF connected along the *a* and *c* axes to the neighboring

TABLE III. Total energy (relative to the lowest energy state in meV f.u.$^{-1}$) for $\mathrm{YBaMn_2O_{5+\delta}}$ and $\mathrm{LaBaMn_2O_{5+\delta}}$ with δ=0, 1/2, and 1 in paramagnetic (P), ferromagnetic (F), and antiferromagnetic (AF) configurations using FPLAPW including GGA and spin-orbit coupling.

Phase	P	F	*A*-AF	*C*-AF	*G*-AF	*a*-SL	*b*-SL	*c*-SL
$\mathrm{YBaMn_2O_5}$	3388	422	125		0			
$\mathrm{LaBaMn_2O_5}$	3421	365.4	220		0			
$\mathrm{YBaMn_2O_{5.5}}$	3090	51.2	58.0	93.2	51.3	84.2	0	67.2
$\mathrm{LaBaMn_2O_{5.5}}$	6268	23.0	54.9	86.7	72.0	268.5	0	62.6
$\mathrm{YBaMn_2O_6}$	1354	83.5	143.8	0	260.1	89.8	128.1	84.2
$\mathrm{LaBaMn_2O_6}$	1220	0	571.5	210.9	625.1	165.9	261.6	265.4

TABLE IV. Calculated and experimental magnetic moments (in μ_B per Mn atom) for $R\mathrm{BaMn_2O_{5+\delta}}$ in the antiferromagnetic ground state (see Table III). Total refers to the total magnetic moment per f.u.

	GGA			GGA+U			Experiment		
Phase	Mn1	Mn2	Total	Mn1	Mn2	Total	Mn1	Mn2	Total
$\mathrm{YBaMn_2O_5}$	2.94	3.79	0.99	3.21	4.06	0.99	2.90[a]	3.90	0.95
$\mathrm{LaBaMn_2O_5}$	2.99	3.88	1.03	2.49	3.49	1.00	2.71[b]	3.21	0.70
$\mathrm{YBaMn_2O_{5.5}}$	3.24	3.36	0.00	3.41	3.49	0.00			
$\mathrm{LaBaMn_2O_{5.5}}$	3.15	3.25	0.00	3.38	3.42	0.00	3.03[c]	3.43	0.00
$\mathrm{YBaMn_2O_6}$	2.86	2.86	0.00	3.20	3.20	0.00			
$\mathrm{LaBaMn_2O_6}$	2.93	2.93	0.00	3.21	3.21	0.00	3.50[b]		

[a]Experimental data from Ref. 3.
[b]Experimental data from Ref. 4.
[c]Experimental data from Ref. 14.

ladders [see Fig. 1(e)]. It may be recalled that the $R\mathrm{BaMn_2O_{5.5}}$ structure has two crystallographically different Mn atoms, which we call Mn1 and Mn2 in Fig. 1. The Mn2-O_b-Mn2 AF interaction in the (100) plane connects half of the Mn atoms of every ladder to the adjacent ladders. In addition, Mn atoms of a particular ladder are AF connected to the upper and lower ladders along [100]. We considered this complex magnetic arrangement, which we designate as the *b*-SL type. In addition, we also considered *a*-SL- and *c*-SL-type arrangements similar to the *b*-SL where the F-spin

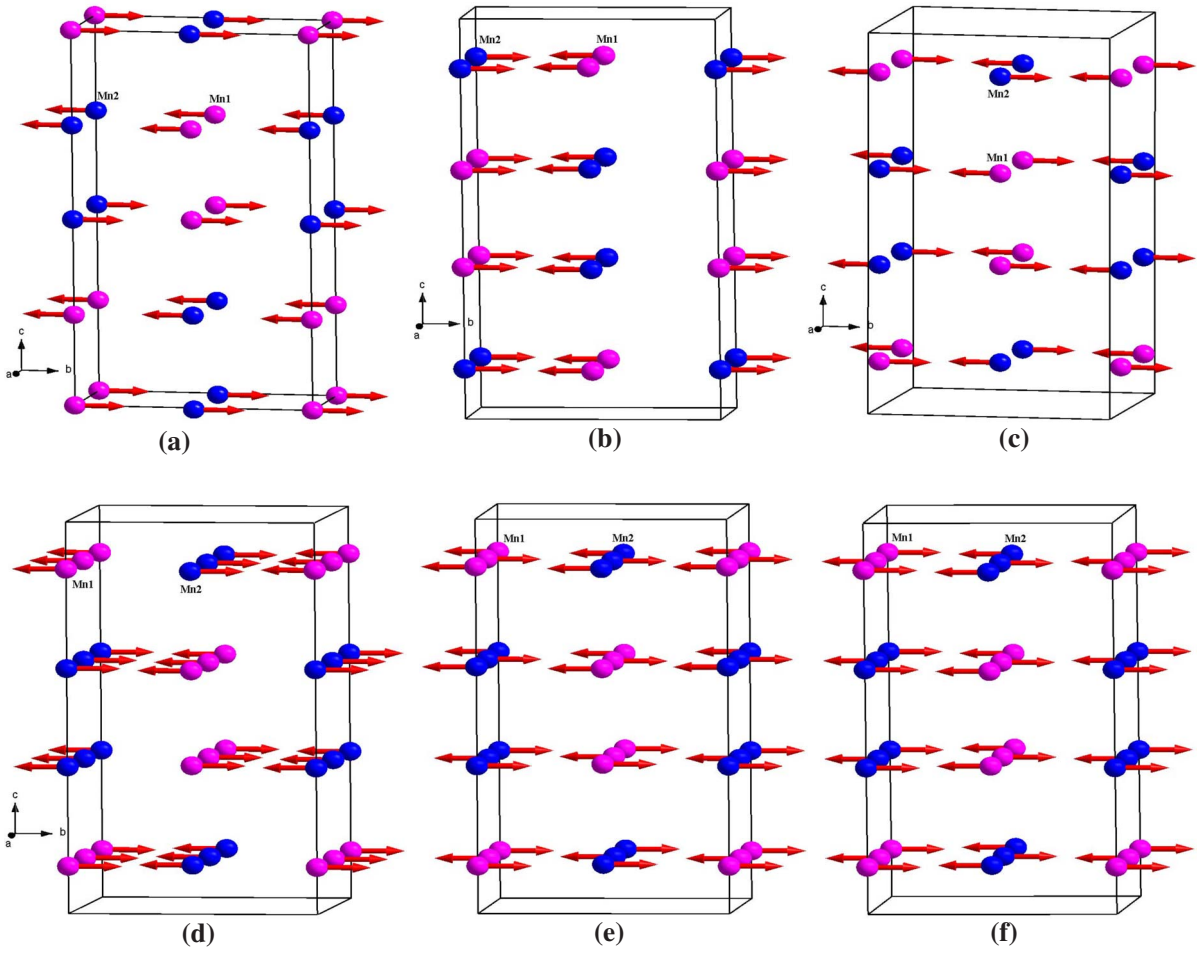

FIG. 1. (Color online) Magnetic configurations considered for $R\mathrm{BaMn_2O_{5.5}}$ and $R\mathrm{BaMn_2O_6}$ in (a) *A*-AF-type, (b) *C*-AF-type, (c) *G*-AF-type, (d) *a*-SL-type, (e) *b*-SL-type, and (f) *c*-SL-type arrangements. Atoms of different crystallographic kinds are labeled on the illustration.

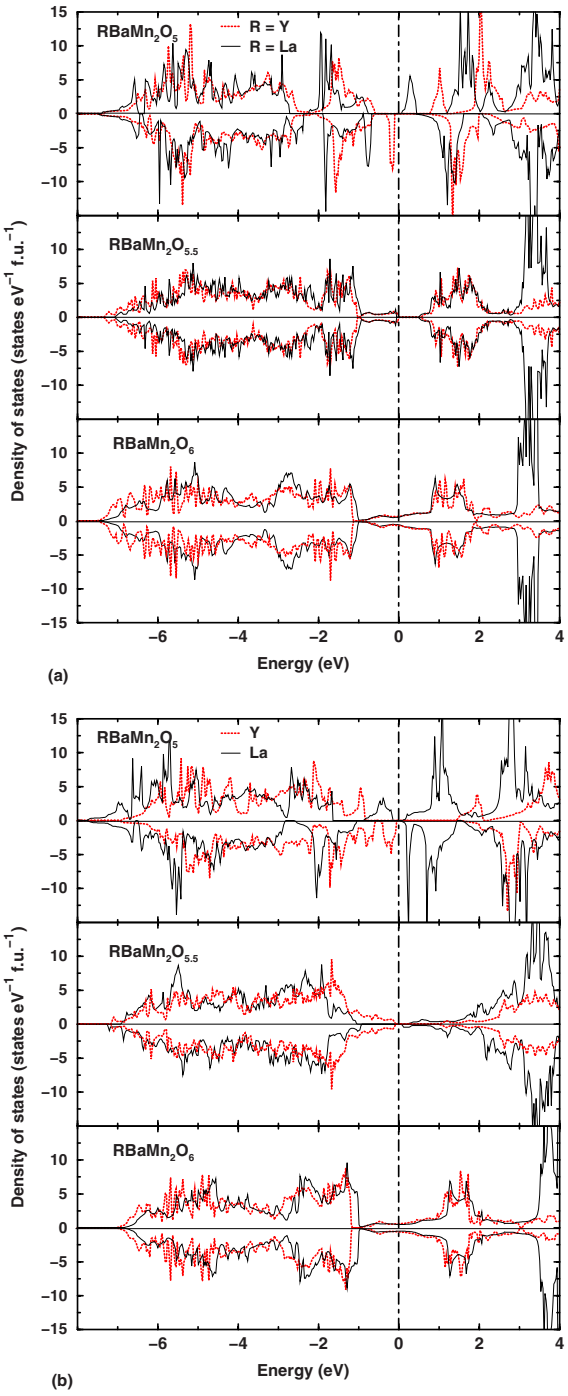

FIG. 2. (Color online) (a) Total density of states (DOS) for RBaMn$_2$O$_{5+\delta}$ with R=Y (red) and La (black) and δ=0, 1/2, and 1 in the ground-state magnetic configurations. (b) Total DOS for the same configurations obtained from GGA+U calculations with U =4.0 eV and J=0.95 eV.

ladders lie along the a and c axes, respectively (AF connected along the other two axes). Moreover, in order to avoid errors introduced by the use of different computational parameters, we have considered F and ferri configurations also in the b-SL-type supercell arrangements. It should be noted that the above-mentioned various AF configurations involve cells with 2–6 f.u. in the calculations. Moreover, noncollinear magnetic structures are indeed possible as the systems contain Mn which is a potential candidate for noncollinearity. However, calculations involving noncollinear magnetic configuration are considered to be outside the scope of the present work.

The total energies obtained after structural optimization (with complete stress and force minimization) shown in Table III clearly indicate that both YBaMn$_2$O$_{5.5}$ and LaBaMn$_2$O$_{5.5}$ take the b-SL-type arrangement as the ground-state magnetic configuration. As the magnetic ground state for LaBaMn$_2$O$_{5.5}$ obtained from the present calculation is in perfect agreement with the experimental magnetic structure[14] as well as with calculations based on the unrestricted Hartree-Fock scheme,[15] there is every reason to believe that YBaMn$_2$O$_{5.5}$ will also take a b-SL-type magnetic configuration, but this needs experimental verifications. The calculated magnetic moments at the Mn sites in YBaMn$_2$O$_{5.5}$ and LaBaMn$_2$O$_{5.5}$ are given in Table IV. The calculated moments for LaBaMn$_2$O$_{5.5}$ are in good agreement with the experimental values. However, the difference between the moments at the two Mn sites obtained using both GGA and GGA+U calculations is not as large as that obtained experimentally.

3. RBaMn$_2$O$_6$

YBaMn$_2$O$_6$ is reported[1] to take an intricately modified CE-AF-type magnetic ordering. Since calculations on this complex magnetic arrangement appeared as a very daunting task, we have only performed structural optimizations for P-, F-, A-, C-, and G-AF-type magnetic arrangements as well as the three different SL-type arrangements (considered for RBaMn$_2$O$_{5.5}$). These calculations involved a minimum of 20 atoms to a maximum of 90 atoms in the magnetic unit cell. Our calculations show that the C-AF-type magnetic configuration has the lowest total energy among the different magnetic arrangements considered. In addition, for YBaMn$_2$O$_6$, we have checked the influence of Coulomb correlation effect on electronic, structural, and magnetic ground states by performing calculations for different U values. In the case of the ground-state monoclinic phase in the C-AF-type magnetic arrangement, the magnetic moment at the Mn site is found to be 3.20, 3.28, and 3.35 μ_B for U=4.0, 5.0, and 6.0 eV, respectively. Similarly, the Mn magnetic moment in the triclinic phase changes from 2.87 through 3.10 to 3.20 μ_B with the corresponding U values.

On the basis of experimental findings, F- and CE-AF-type states are believed[16] to coexist for LaBaMn$_2$O$_6$ at low temperatures. Our structural optimizations show that the F state has the lowest energy among the different magnetic configurations considered. A Curie temperature (T_C) of 335 K is experimentally reported[16] for LaBaMn$_2$O$_6$. Our earlier[2] total-energy calculations based on the full-potential linear muffin-tin orbital[17] method have shown that this phase should take an AF ground state. As we did not perform structural optimization on the earlier occasion and the energy difference between F and C-AF configurations is very small, the coexistence of F and AF states may be possible. However, calculations on an explicit CE-AF-type state may be able to resolve this issue.

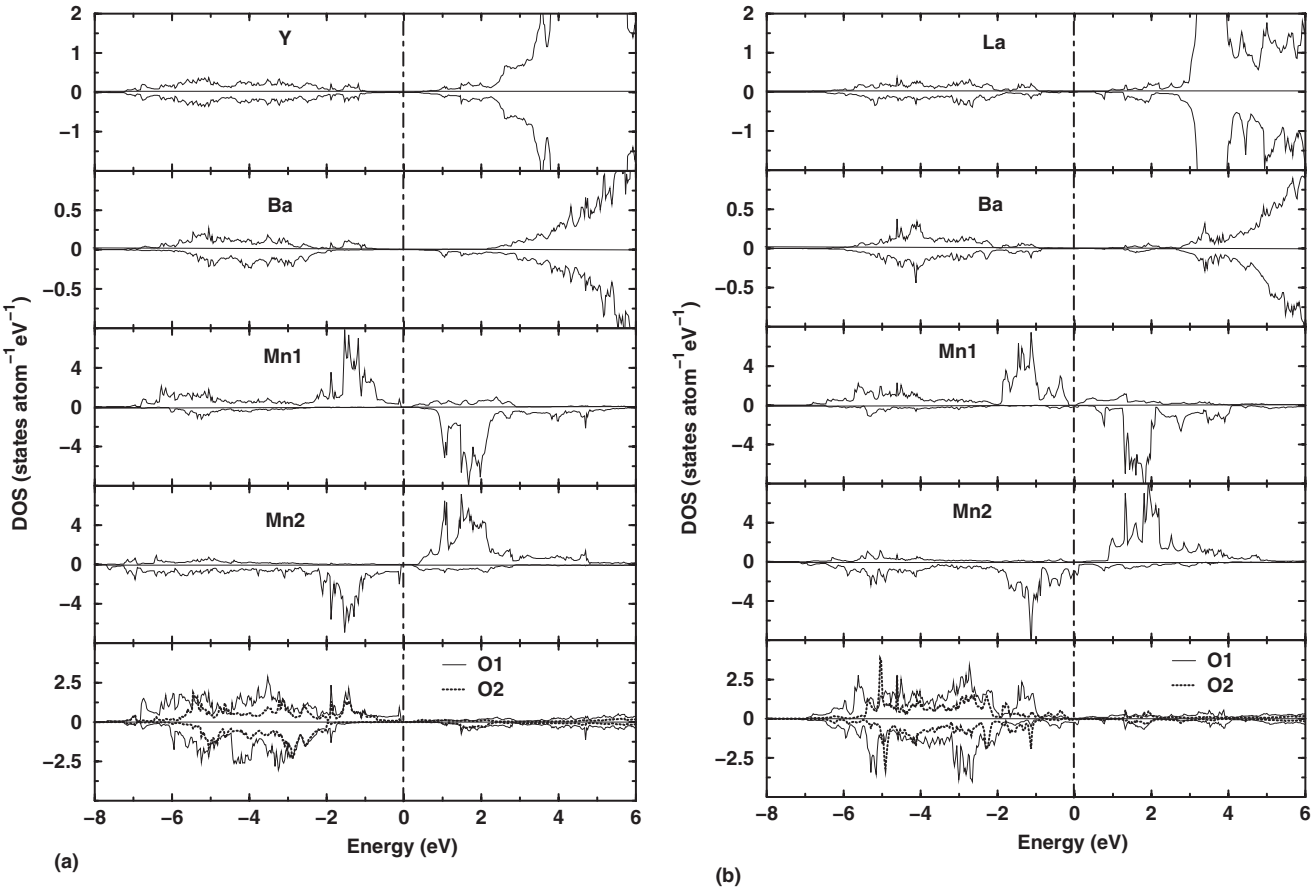

FIG. 3. Site-projected density of states (DOS) for $R\mathrm{BaMn_2O_{5.5}}$ with R=(a) Y and (b) La in appropriate antiferromagnetic configurations.

The calculated orbital moments are negligible ($\sim$0.01–0.02 μ_B per Mn atom) in the phases studied here. Table IV shows that the difference between the magnetic moments at the Mn1 and Mn2 sites decreases gradually on increasing δ from 0 to 1/2. Differences in magnetic moments are commonly used as an indicator for different valence states. The magnetic moment data alone suggest different valence states for Mn at δ=0 and valence equalization at δ=1/2 and 1. A detailed analysis of the electronic structure parameters shows that the situation is not so simple (see below). However, it seems safe to conclude that cooperative magnetic properties are mainly determined by the oxygen content of these phases rather than by the size and other features associated with Y and/or La.

From the calculated magnetic moments, we infer that the Mn atoms in $R\mathrm{BaMn_2O_5}$ can be categorized as belonging to the class-I mixed-valence (MV)[18] configuration where the Mn sites take different charge states. When the oxygen content is increased to δ=1/2, the Mn atoms can be regarded as converted to the class-II MV category where two different charge states are still maintained but with only a slight difference between them. On the other hand, when the oxygen atoms completely fill the R layer, the Mn atoms may convert to the class-III MV category where the distinctions in coordination and charge states have completely disappeared. In $\mathrm{YBaFe_2O_5}$,[19] the conversion from class-III to class-II and finally to class-I MV situation has been demonstrated to occur on decreasing temperature. However, in the present case, we witness that such a conversion takes place on changing the oxygen stoichiometry. In general, one can expect such behaviors in various perovskitelike oxides as a function of electron or hole doping.

C. Electronic structure

1. $R\mathrm{BaMn_2O_5}$

The electronic structures of the studied phases are analyzed in terms of total as well as site- and orbital-projected density of states (DOS) representations. The higher-energy P state of the $R\mathrm{BaMn_2O_5}$ phases exhibits a metallic character with a finite number of states at the Fermi level (E_F). The F state also exhibits a metallic behavior but with a small number of states at the E_F. The total DOSs of $R\mathrm{BaMn_2O_{5+\delta}}$ in the ground-state configurations are displayed in Fig. 2(a). The $R\mathrm{BaMn_2O_5}$ phases are semiconducting with energy gaps of 0.88 and 0.86 eV for R=Y and La, respectively. The total DOSs obtained from GGA+U calculations are shown in Fig. 2(b). According to this approach, the band gap for $\mathrm{YBaMn_2O_5}$ is increased to 1.49 eV, whereas that for $\mathrm{LaBaMn_2O_5}$ is surprisingly decreased to 0.32 eV. The filling up of the originally unoccupied Mn1 d_{xy} orbital may be the reason for the reduction in the magnetic moment at the Mn1

site and the decreased band gap. Since the site-projected DOSs for the RBaMn$_2$O$_5$ phases are reported already in Refs. 2 and 5, we only briefly recapitulate the main features.

An almost empty valence band (VB) situation for the R and Ba constituents and a completely filled VB for the O atoms indicate that R and Ba have donated their valence electrons mainly to the O atoms and themselves become cationic species. The VB mainly consists of Mn d and O p states. The Mn d states for the two crystallographically different Mn atoms have different topologies, which signals different valence and/or charge states for Mn in the RBaMn$_2$O$_5$ phases.

2. RBaMn$_2$O$_{5.5}$

In the higher-energy P state, the RBaMn$_2$O$_{5.5}$ phases also have a metallic character. In the F state, YBaMn$_2$O$_{5.5}$ exhibits a semiconducting behavior with a 0.24 eV gap in the majority-spin channel and a 2.12 eV gap in the minority-spin channel. On the other hand, LaBaMn$_2$O$_{5.5}$ exhibits a half-metallic behavior with a finite number of states at the E_F in the majority-spin channel and an energy gap of 1.83 eV in the minority-spin channel. In the ground-state b-SL-type AF configuration, both the R=Y and La phases have a semiconducting behavior with a band gap of 0.58 eV for YBaMn$_2$O$_{5.5}$ and 0.54 eV for LaBaMn$_2$O$_{5.5}$. In the higher-energy C-AF-type configurations, YBaMn$_2$O$_{5.5}$ and LaBaMn$_2$O$_{5.5}$ show energy gaps of 0.22 and 0.26 eV, respectively. Increased band gaps in the ground state (b-SL type) of the RBaMn$_2$O$_{5.5}$ phases may be indicative of the increased stability of these systems. The band gaps of YBaMn$_2$O$_{5.5}$ and LaBaMn$_2$O$_{5.5}$ increase to 1.25 and 0.95 eV, respectively, on the introduction of Coulomb correlation effects. Since simple GGA calculations are themselves able to bring out the semiconducting behavior, we explore the finer details of the electronic structure by this method.

From Fig. 3, it is evident that the R and Ba atoms have largely donated their valence electrons to the other constituents and themselves entered into nearly pure ionic states (evident from the small number of states in the VB and a larger number of states in the conduction band). It can be recalled that in the phases with δ=1/2, Mn1 is associated with the square-pyramidal coordination and Mn2 with the octahedral coordination. Thus, the two Mn atoms adopt different topologies of DOS profiles for YBaMn$_2$O$_{5.5}$ as well as for LaBaMn$_2$O$_{5.5}$. This implies that different valence and/or charge states can be expected for the two different Mn atoms in these phases. Although Mn d states are seen from −7 eV to E_F, the most prominent d states are localized from −2 eV to E_F for both phases. The degree of localization is comparatively larger for Mn2 than that for Mn1 in both YBaMn$_2$O$_{5.5}$ and LaBaMn$_2$O$_{5.5}$. This may give a hint why the magnetic moment at Mn2 is slightly larger than that at Mn1. Most of the oxygen states are found in the range −7 to −1 eV for both phases. Since the Mn and O states cover more or less the same energy range, there must occur an appreciable hybridization and a significant degree of Mn-O covalent bonding character.

3. RBaMn$_2$O$_6$

Similar to the RBaMn$_2$O$_{5.5}$ phases, YBaMn$_2$O$_6$ exhibits a metallic behavior in the P state and a half-metallic character

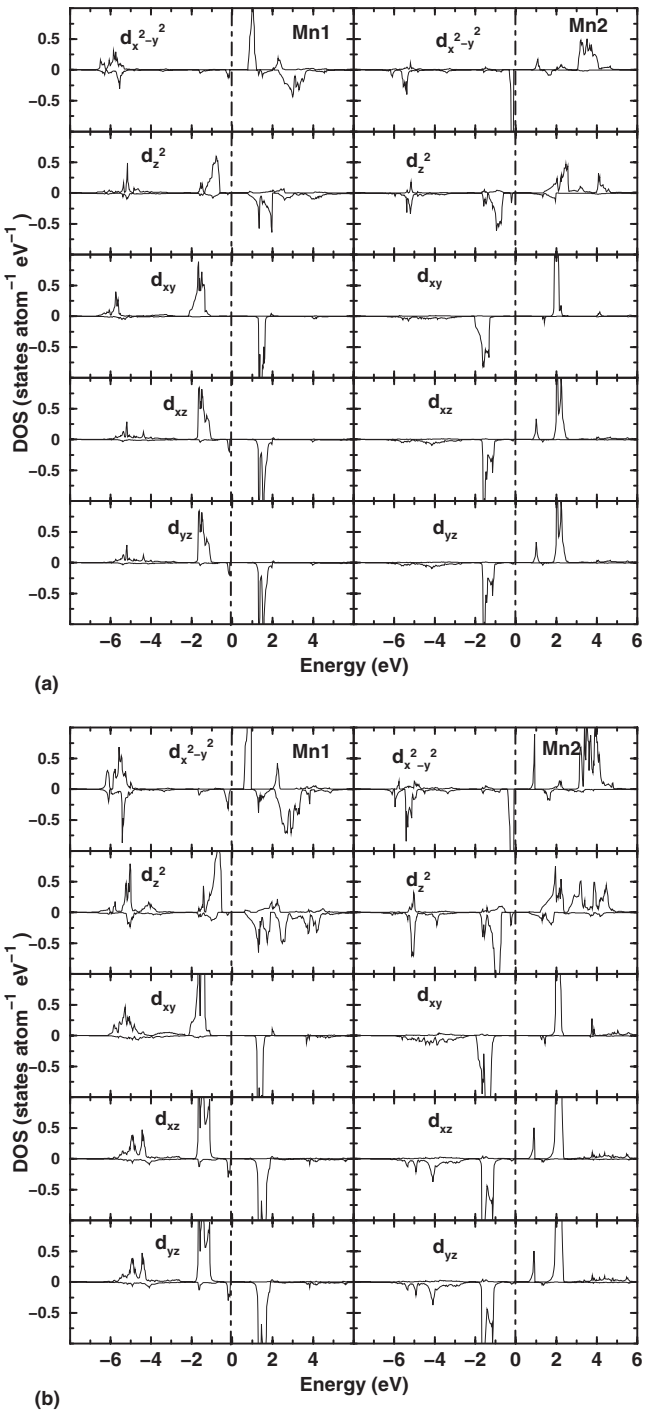

FIG. 4. The d-orbital-projected density of states for (a) YBaMn$_2$O$_5$ and (b) LaBaMn$_2$O$_5$ in the ground-state ferrimagnetic configurations.

in the higher-energy F state with an energy gap in the minority-spin channel of 1.61 eV. The decrease in the gap on going from δ=0 to 1 would in itself be an indication of the increase in covalent bonding interaction between Mn d and O p states by the increase in oxygen stoichiometry.

In the ground-state AF configuration, the band gap has completely disappeared and a finite number of states is clearly seen at the E_F in Fig. 2 for YBaMn$_2$O$_6$. The states at

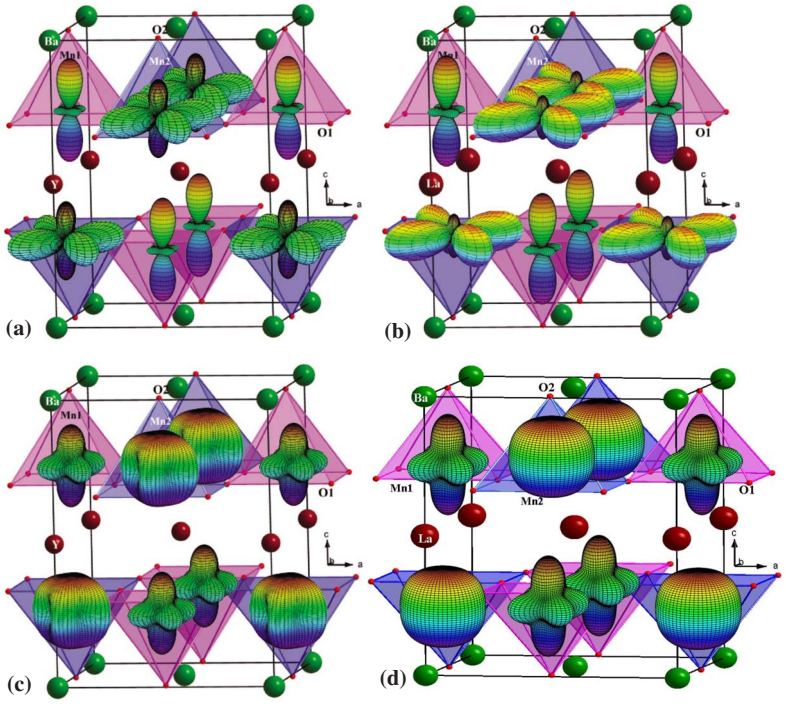

FIG. 5. (Color online) Orbital ordering pattern obtained from the occupation-density matrices of *d* states close to the Fermi level in (a) $YBaMn_2O_5$ and (b) $LaBaMn_2O_5$. Charge ordering pattern obtained from the occupation-density matrices for majority-spin *d* orbitals in the entire valence band in (c) $YBaMn_2O_5$ and (d) $LaBaMn_2O_5$. Purple-colored (light gray) polyhedra contain Mn1 and blue-colored (dark gray) polyhedra contain Mn2 as central atoms. The degree of filling of *d* orbitals is indicated by the radial extension of the orbitals.

or near the E_F originate from Mn *d* and O *p* orbitals, which implies that the enhanced hybridization interaction between the electrons concerned leads to the increased metallic character. It is worthwhile to recall that the $YBaMn_2O_6$ structure comprises highly distorted octahedra compared to those in $LaBaMn_2O_6$ due to the large size mismatch between Y and Ba. Moreover, the oxygen atoms in the "base planes" of the coordination polyhedra become gradually more displaced toward the Y layers with increasing δ. Thereby, the corresponding Mn-O distances are decreased and the hybridization interaction increased and so does the number of states at the E_F.

For the phases with $\delta=0$ and $1/2$, we found that the GGA with spin-orbit coupling is able to provide the correct insulating behaviors and magnetic ground states. Hence, we had expected the same outcome for the $R\mathrm{BaMn_2O_6}$ phases. Fair enough, our calculations gave magnetic ground states for these compounds closer to experiments, but with a metallic rather than an insulating behavior. Note that Nakajima *et al.*[1] claimed successive phase transitions for $YBaMn_2O_6$ from a P-metallic state via a P-insulating state to an AF-insulating state. We have even compared DOS profiles for these phases in the various magnetic configurations that have been considered for structural optimization. However, metallic rather than insulating electronic structure behavior is retained for all magnetic configurations considered. This result may of course be an indication for stronger correlation effects than anticipated. Therefore, as a natural extension of our examinations of these phases, we tried to account for correlation effects by performing GGA+*U* calculations.

Interestingly, both the $R\mathrm{BaMn_2O_6}$ phases continue to display a metallic behavior despite the inclusion of Coulomb correlation effects in the calculations. It can be seen from Sec. III B that the magnetic moments of Mn increase on increasing the *U* values from 4.0 to 6.0 eV for the monoclinic as well as the triclinic variants of $YBaMn_2O_6$. Even though the increase in magnetic moments indicates increased localization of Mn *d* states, the electronic structure still displays a metallic character, implying its robustness with regard to the variation of *U*. So, we believe that the experimentally observed insulating behavior of the $R\mathrm{BaMn_2O_6}$ phases may not be associated with the Coulomb correlation effects but with a more complex magnetic ordering which is not considered in the present calculations. It may be recalled that, in the case of $LaMnO_3$,[20] we only obtained the correct insulating ground state when the experimentally established *A*-AF-type configuration was taken into account in the calculations. Hence, we believe that one may also obtain an insulating behavior for the $R\mathrm{BaMn_2O_6}$ phases on including the experimentally inferred *CE*-AF-type ordering in the calculations.

The oxygen-filled-up $R\mathrm{BaMn_2O_6}$ phases do not have very different site-projected DOS profiles. The DOS features for these phases (not shown) are similar to those for $\delta=0$ and $1/2$ in the sense that *R* and Ba have few states in the VB and accordingly appreciable ionic character. The metallic conductivity of $R\mathrm{BaMn_2O_6}$ mainly originates from the Mn *d* states. The most prominent localized Mn states are found close to E_F (from -2 to -1 eV), whereas more dispersed states are found from -7 to -2 eV. The oxygen atoms of the two phases also have prominent states in the same energy range (-7 to -2 eV), again evidencing covalent bonding interaction between the Mn and O atoms. It is interesting to note that more Mn *d* and O *p* states are present at the E_F for $YBaMn_2O_6$ than for $LaBaMn_2O_6$. This implies a stronger covalent interaction between Mn and O atoms in the former phase, thus reducing the magnetic moments at Mn compared to the latter phase.

A closer inspection of the total DOS curves reveals that the overall electronic structure features within the VB are

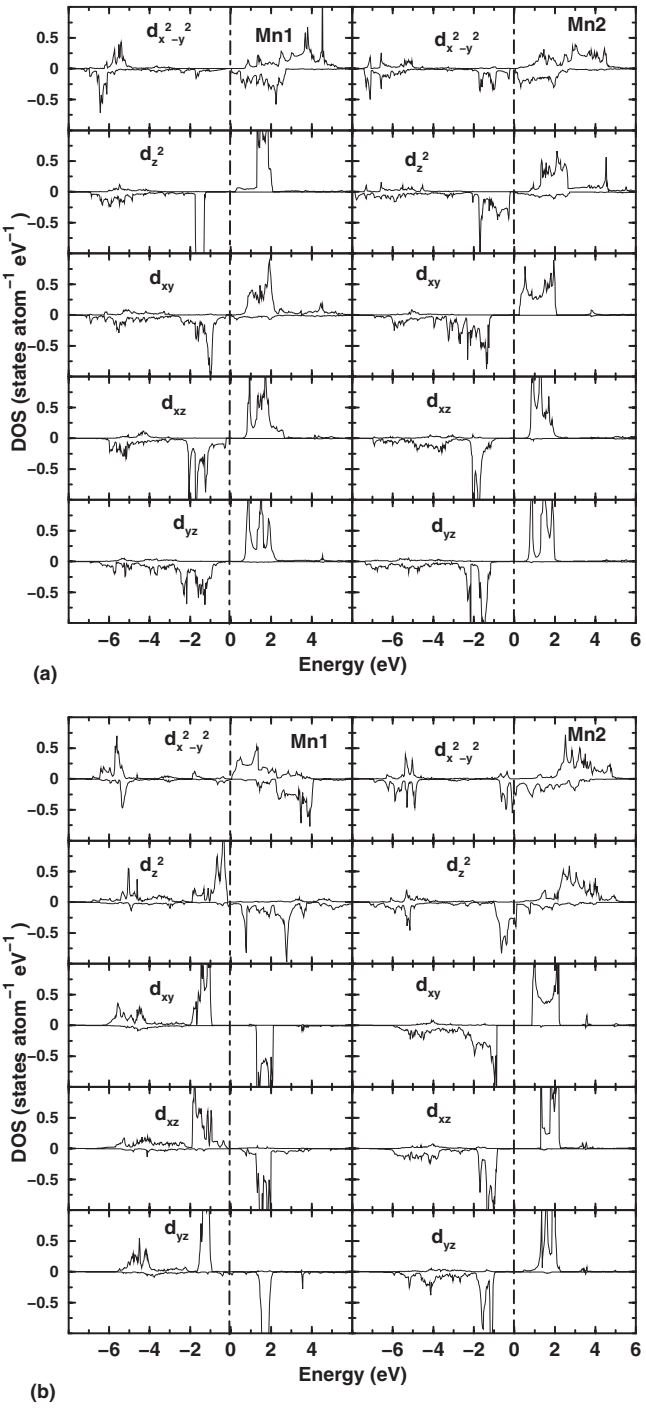

FIG. 6. The d-orbital-projected density of states for (a) YBaMn$_2$O$_{5.5}$ and (b) LaBaMn$_2$O$_{5.5}$ in the antiferromagnetic configurations.

similar for the Y and La variants. In the case of RBaMn$_2$O$_5$, a small band gap is seen around −2.2 eV, but this is converted to a small valley (psuedo-gap-like) feature around −2 eV in RBaMn$_2$O$_{5.5}$ phases. This gap has completely disappeared in RBaMn$_2$O$_6$, which instead shows a gap around −1 eV. Hence, it can be concluded that the oxygen content plays an important role in deciding not only the crystal structure but also the electronic structure. On the other hand, the effect of the size of R is minimal on the main features of the electronic structure. However, the finer details of the electronic structure also depend on the Mn-O-Mn bond angles which are determined by the size of the R constituents. In fact, we will show below that the cation-size effect plays an important role in the OO and consequently on the magnetic properties via the exchange interaction.

D. Orbital and charge ordering

1. RBaMn$_2$O$_5$

As the electrons in the vicinity of the E_F participate in hopping and hence in exchange interactions, we have projected these electrons to visualize the OO patterns. In our earlier report,[2] we determined the OO pattern for LaBaMn$_2$O$_5$ from its orbital-projected DOS. The presence of d_{xy}, d_{xz}, and d_{yz} orbitals close to E_F has led us to believe that these orbitals are responsible for the OO in LaBaMn$_2$O$_5$. In the present study, we make use of the energy-projected occupation-density matrix to evaluate the CO and OO. From this modified approach, we are not only able to identify the occupation of a particular orbital in a particular energy range but we also obtain the orbital orientation. Hence, we believe that this approach may be more appropriate to visualize the OO features. According to this procedure, we find no significant difference between the OO patterns of YBaMn$_2$O$_5$ and LaBaMn$_2$O$_5$ [see Figs. 5(a) and 5(b)]. The d-orbital-projected DOS (Fig. 4) for the RBaMn$_2$O$_5$ phases display almost similar features in the sense that the d_{z^2} orbital on Mn1 and d_{z^2} and $d_{x^2-y^2}$ orbitals on Mn2 occur close to the E_F. Therefore, these orbitals order in both RBaMn$_2$O$_5$ phases according to a pattern named[13] as F-orbital order [Fig. 5(a) and 5(b)], viz., the same pattern as established for OO in YBaMn$_2$O$_5$ and LaBaMn$_2$O$_5$. As the degree of filling of the $d_{x^2-y^2}$ orbital on Mn2 in LaBaMn$_2$O$_5$ is slightly larger than that in YBaMn$_2$O$_5$, the radial distribution of this orbital is depicted as considerably larger in Fig. 5(b).

It can be recalled that the d orbitals on Mn atoms in square-pyramidal coordination are splitted into doubly degenerate e_g (d_{xz},d_{yz}) and nondegenerate b_{2g} (d_{xy}), a_{1g} (d_{z^2}), and b_{1g} ($d_{x^2-y^2}$) levels.[22] As four of the five d orbitals are singly occupied, Mn1 can be formally assigned an Mn^{3+} (d^4); high-spin (HS) state. Likewise, Mn2 has all d orbitals singly occupied, which prompts a formal assignment as Mn^{2+} (d^5;HS) for Mn2 in the RBaMn$_2$O$_5$ phases. The average values of the diagonal components of the Born-effective-charge tensor for the Mn atoms[23] also reinforce this assignment. The ordering of the $d_{x^2-y^2}$ orbital on Mn2 elongates the Mn2-O$_b$ bond length along the ab plane. Moreover, the atomic arrangements of the RBaMn$_2$O$_5$ phases have Mn-O$_b$-Mn bond angles deviating from 180° in the square-pyramid base plane, which hinder the transfer of electrons and tend to localize more electrons on the Mn2 site than on the Mn1 site, thereby leading to a CO state. As each Mn atom is surrounded by five aliovalent Mn atoms as nearest neighbors, a checkerboard-type CO is established [see Figs. 5(c) and 5(d)] for RBaMn$_2$O$_5$ phases.

2. RBaMn$_2$O$_{5.5}$

When the oxygen atoms half fill the R layer in the $\delta = 1/2$ phases, half of the square pyramids have become oc-

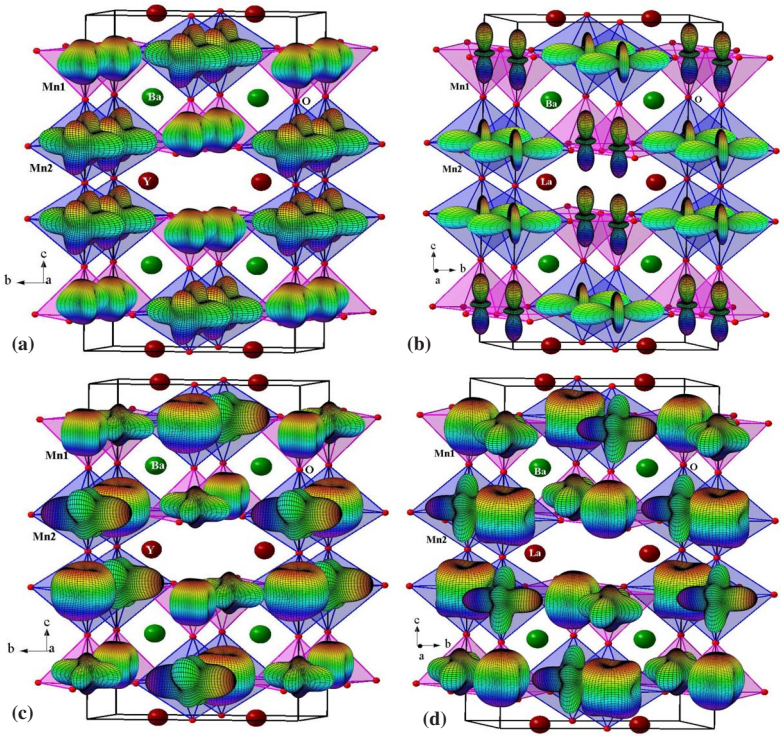

FIG. 7. (Color online) Orbital ordering patterns obtained from the occupation-density matrices of d states close to the Fermi level in (a) $YBaMn_2O_{5.5}$ and (b) $LaBaMn_2O_{5.5}$. Charge ordering pattern obtained from the occupation-density matrices of majority-spin d orbitals in the entire valence band is shown in (c) $YBaMn_2O_{5.5}$ and (d) $LaBaMn_2O_{5.5}$. Purple-colored (light gray) polyhedra contain Mn1 and blue-colored (dark gray) polyhedra contain Mn2 as central atoms. The degree of filling of d orbitals is indicated by the radial extension of the orbitals.

tahedra. Owing to the oxygen vacancies still present in the R layers, strain in the $R\mathrm{MnO}_{2.5}$ layer induces short Mn2-O_a (apical) distances along the c direction. At the same time, stretching of the $BaMnO_3$ layer produces long Mn1-O_a distances. Consequently, JTD of the Mn2 octahedra extends along [010] and this perturbation plays[14] an important role for the OO patterns in $YBaMn_2O_{5.5}$ and $LaBaMn_2O_{5.5}$.

According to the features of orbital-projected DOS (Fig. 6), the d_{xy}, d_{yz}, and some d_{xz} states have significant presence close to E_F. Thus, these orbitals determine the OO on Mn1 in $YBaMn_2O_{5.5}$. On the other hand, mainly d_{z^2} together with a few $d_{x^2-y^2}$ states are predominantly present close to E_F on Mn2 and accordingly these orbitals determine OO at this site. However, due to the JTD, the d_{z^2} ($d_{3y^2-r^2}$) orbital is rotated and lies along the b axis. This is one of the reasons why the Mn2-O_b bonds are longer than the Mn1-O_b bonds. The corresponding OO patterns in the $YBaMn_2O_{5.5}$ phase are displayed in Fig. 7(a). The ordering of the d_{z^2} orbital on Mn1 in $LaBaMn_2O_{5.5}$ along the c axis elongates the Mn1-O_a bonds. The states close to E_F on Mn2 have a predominantly d_{z^2} character together with a certain weft of a $d_{x^2-y^2}$ character. Similar to the case in $YBaMn_2O_{5.5}$, the d_{z^2} orbital is rotated to occur along the b axis [Fig. 7(b)] due to the JTD effect, thus elongating the Mn2-O_b bonds compared to the Mn2-O_a bonds. It may be noted that even though the overall electronic-structure features are almost similar for $YBaMn_2O_{5.5}$ and $LaBaMn_2O_{5.5}$, the difference in OO patterns leads to a different degree of distortion of the coordination polyhedra in the R=Y and La phases.

In spite of the fact that the OO patterns exhibit noticeable differences in the $YBaMn_2O_{5.5}$ and $LaBaMn_2O_{5.5}$ phases, the degree of filling of the VB is same for both phases. This can be inferred from the CO patterns (displayed by the filling of majority-spin channel) in Figs. 7(c) and 7(d). As pointed out earlier, the degree of structural distortion is larger in $YBaMn_2O_{5.5}$ than that in $LaBaMn_2O_{5.5}$ phase. However, the similar degree of filling of VB in both phases is associated with the same valence states of constituents in both phases. Owing to the different types of Mn-O coordinations and the associated differences in bond distances and angles for the Mn atoms, the charges localize on the Mn sites and leads to a CO state. Figures 7(c) and 7(d) show the so-called stripe-type CO patterns in $YBaMn_2O_{5.5}$ and $LaBaMn_2O_{5.5}$.

3. $R\mathrm{BaMn}_2\mathrm{O}_6$

Even though two distinct crystallographic Mn sites have been identified for $YBaMn_2O_6$, the calculated magnetic moments are the same (see Table IV). Hence, the two Mn atoms are supposed to be in the same charge state. According to the formal valence counting for Mn^{3+};HS, three electrons should singly occupy the triply degenerate t_{2g} levels and one electron should occupy one of the doubly degenerate e_g levels. On the other hand for Mn^{4+};HS, the t_{2g} orbitals should be singly occupied, leaving the two e_g orbitals empty. However, the orbital-projected DOS (Fig. 8) for $R\mathrm{BaMn}_2\mathrm{O}_6$ phases do not exhibit such features. On the contrary, all five d orbitals have noticeable states in the VB. Hence, Mn in these phases can be coarsely assigned an average $Mn^{3.5+}$ charge state. A relatively large amount of DOS close to the E_F is seen for the $d_{x^2-y^2}$ and d_{z^2} orbitals at the Mn sites of $YBaMn_2O_6$. Therefore, these orbitals order on the Mn atoms [see Fig. 9(a)]. The large deviations from 180° of the Mn-O_b-Mn bond angles along the base plane of the octahedra are believed to obstruct the transfer of charges leading to their localization in different ordering patterns. As a result of the JTD, the d_{z^2} orbital on the Mn1 site is believed to exhibit F-OO according to the experiment.[13] A possible OO of the $d_{x^2-y^2}$ orbital has

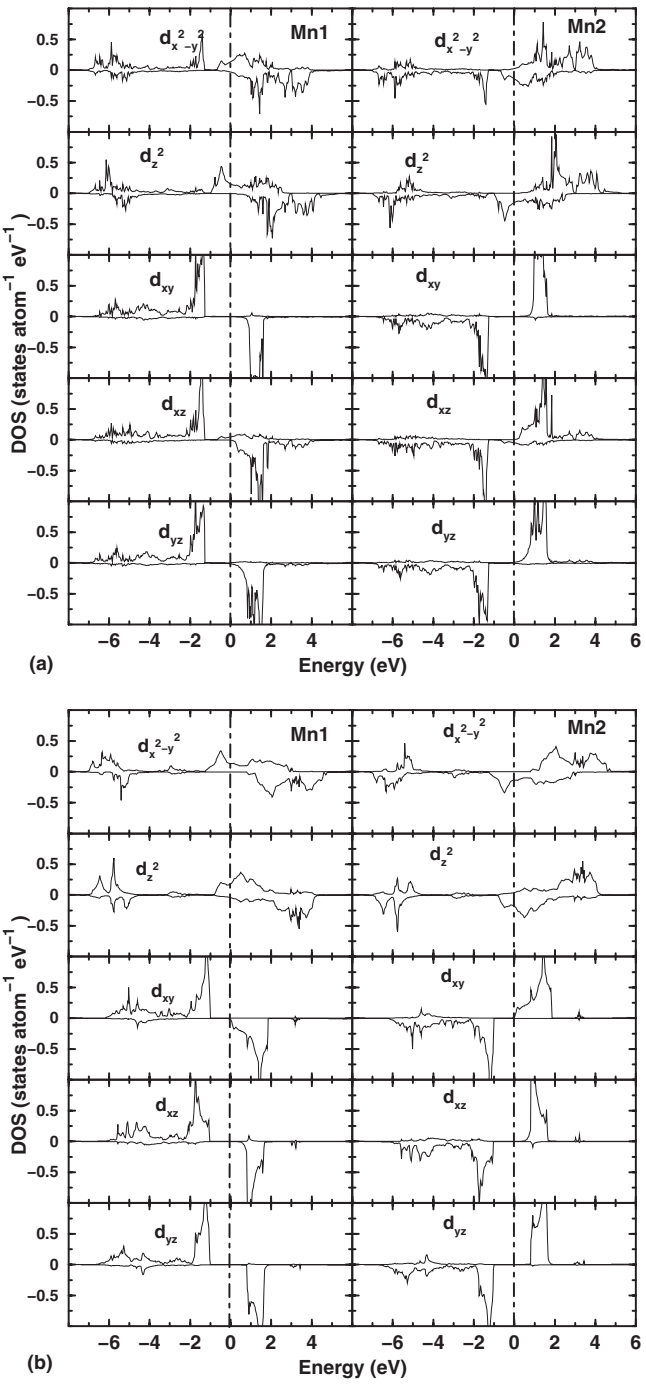

FIG. 8. The d-orbital-projected density of states for (a) YBaMn$_2$O$_6$ and (b) LaBaMn$_2$O$_6$ in the antiferromagnetic configurations.

been suggested by Nakajima *et al.*[21] As the ordering pattern is same at the Mn sites, it may be classified as belonging to the F-OO type. The orbital-projected DOS for LaBaMn$_2$O$_6$ [Fig. 8(b)] shows that the d_{z^2} and $d_{x^2-y^2}$ orbitals at the Mn sites occur close to E_F. Therefore, the ordering of these orbitals manifest themselves as spherical distributions [Fig. 9(b)].

The CO on the Mn sites in YBaMn$_2$O$_6$ and LaBaMn$_2$O$_6$ is displayed in Figs. 9(c) and 9(d). In the case of YBaMn$_2$O$_6$, there is a small difference between the ordered charges on Mn1 and Mn2, whereas for LaBaMn$_2$O$_6$, only a spherical distribution of charges is seen without any special ordering pattern. However, it should be remembered that our calculations on the RBaMn$_2$O$_6$ phases indicate a metallic character. Hence, charge localization, one of the main requirements for CO, should be absent in these phases. Experimental work on YBaMn$_2$O$_6$ reports[1] a metal-to-insulator transition below 230 K and a modified-*CE*-type CO. Even though our calculations show some indications for CO in YBaMn$_2$O$_6$, its metallic character shrouds this interpretation in a cloud of uncertainty. Therefore, the calculations on the experimentally suggested modified-*CE*-AF-type structure becomes mandatory in order to establish the properties of these phases more correctly. Until such calculation come at hand, our findings on these phases should be regarded as qualitative and significance should not be attached to the finer details of the band structure.

IV. CONCLUSIONS

In order to evaluate the combined effect of oxygen content and size of the R constituents on spin, charge, and orbital orderings, accurate electronic-band structure calculations have been carried out on RBaMn$_2$O$_{5+\delta}$ (R=Y, La; δ=0, 1/2, 1). Full-potential linearized-augmented plane-wave methods have been employed for the study. Structural optimizations (stress and force minimizations) have been performed considering various possible magnetic orderings for the RBaMn$_2$O$_{5+\delta}$ phases. The structural parameters obtained from such calculations are found to be in good agreement with the experimental values. While ferrimagnetic ground states have been correctly established for the RBaMn$_2$O$_5$ phases, an experimentally inferred spin-ladder arrangement along the b direction for LaBaMn$_2$O$_{5.5}$ has been correctly reproduced by our calculations. Similarly, the magnetic structure for YBaMn$_2$O$_{5.5}$ is predicted to be the same as that of LaBaMn$_2$O$_{5.5}$. Among the various magnetic orderings, *C*-AF-type and ferromagnetic configurations are found to have the lowest energy for YBaMn$_2$O$_6$ and LaBaMn$_2$O$_6$, respectively. The calculated magnetic moments are found to be in close agreement with available experimental data. The studied phases are seen to undergo gradual changes from so-called class-I via class-II to class-III mixed-valence situations on increasing the oxygen content from δ=0 via 1/2 to 1. The electronic structure is also found to vary from insulator to metal on going from δ=0 to 1, with a decreased band gap for the intermediate δ=1/2 phases. The RBaMn$_2$O$_6$ phases are reported to be insulating from experimental studies; in order to bring out this feature in the computational treatment, one needs to include the correct cooperative magnetic order in the calculations.

The overall physical properties such as magnetic and electronic properties change as a function of the oxygen content. The influence of the oxygen content on the Mn-O framework together with valence changes appears to be the origin of this relationship, notably through facilitation or obstruction of charge transfer and/or exchange interactions. We have also established that the size of R constituent plays a role in de-

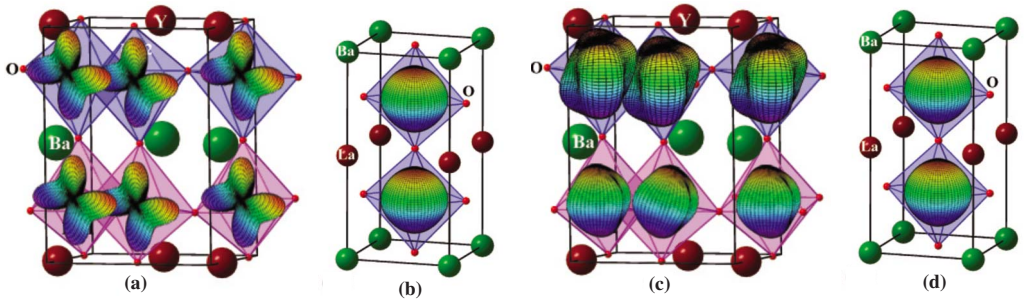

FIG. 9. (Color online) The *d*-orbital-projected density of states for (a) $YBaMn_2O_6$ and (b) $LaBaMn_2O_6$. The charge ordering pattern obtained from the occupation-density matrices of majority-spin *d* orbitals in (c) $YBaMn_2O_6$ and (d) $LaBaMn_2O_6$. The purple-colored polyhedra contain Mn1 and blue-colored polyhedra contain Mn2 as central atoms. The degree of filling of *d* orbitals is indicated by their radial extension.

termining the shape and the related distortions of the coordination polyhedra such as elongation or shortening of particular Mn-O bond(s), which in turn influences the occupancy or vacancy of a particular *d* orbital(s). Therefore, intricate details of charge and orbital ordering (such as occupation of a particular orbital in a particular energy range and the associated orbital ordering) are found to vary with the size of the *R* constituent.

ACKNOWLEDGMENTS

R.V. and P.R. kindly acknowledge Karel Knizek for useful communications. The authors are grateful to the Research Council of Norway for financial support. Part of these calculations was carried out on the Norwegian supercomputer facilities.

*vidya.ravindran@kjemi.uio.no

[1] T. Nakajima, H. Kageyama, M. Ichihara, K. Ohoyama, H. Yoshizawa, and Y. Ueda, J. Solid State Chem. **177**, 987 (2004).
[2] R. Vidya, P. Ravindran, P. Vajeeston, A. Kjekshus, and H. Fjellvåg, Phys. Rev. B **69**, 092405 (2004).
[3] F. Millange, E. Suard, V. Caignaert, and B. Raveau, Mater. Res. Bull. **34**, 1 (1999).
[4] F. Millange, V. Caignaert, B. Domenges, and B. Raveau, Chem. Mater. **10**, 1974 (1998).
[5] R. Vidya, P. Ravindran, A. Kjekshus, and H. Fjellvåg, Phys. Rev. B **65**, 144422 (2002).
[6] P. Blaha, K. Schwarz, G. K. H. Madsen, D. Kvasnicka, and J. Luitz, WIEN2K, revised edition, an augmented plane wave +local orbital program for calculating crystal properties, Vienna University of Technology, 2001.
[7] P. E. Blöchl, Phys. Rev. B **50**, 17953 (1994).
[8] J. P. Perdew, S. Burke, and M. Ernzerhof, Phys. Rev. Lett. **77**, 3865 (1996).
[9] V. I. Anisimov, I. V. Solevyev, M. A. Korotin, M. T. Czyzyk, and G. A. Sawatzky, Phys. Rev. B **48**, 16929 (1993).
[10] P. Novak, F. Boucher, P. Gressier, P. Blaha, and K. Schwarz, Phys. Rev. B **63**, 235114 (2001).
[11] G. Kresse and J. Furthmuller, Comput. Mater. Sci. **6**, 15 (1996).
[12] M. Karppinen, H. Okamoto, H. Fjellvåg, T. Motohashi, and H. Yamauchi, J. Solid State Chem. **177**, 2122 (2004).
[13] A. J. Williams and J. P. Attfield, Phys. Rev. B **72**, 024436 (2005).
[14] V. Caignaert, F. Millange, B. Domenges, B. Raveau, and E. Suard, Chem. Mater. **11**, 930 (1999).
[15] Q. Zhang, W. Zhang, and Z. Jiang, Phys. Rev. B **72**, 144415 (2005).
[16] T. Nakajima, H. Kageyama, H. Yoshizawa, and Y. Ueda, J. Phys. Soc. Jpn. **71**, 2843 (2002).
[17] J. M. Wills, O. Eriksson, M. Alouani, and D. L. Price, in *Electronic Structure and Physical Properties of Materials*, edited by H. Dreysse (Springer, Berlin, 2000), p. 148; J. M. Wills and B. R. Cooper, Phys. Rev. B **36**, 3809 (1987); D. L. Price and B. R. Cooper, *ibid.* **39**, 4945 (1989).
[18] M. B. Robin and P. Day, Adv. Inorg. Chem. Radiochem. **10**, 247 (1967).
[19] P. M. Woodward and P. Karen, Inorg. Chem. **42**, 1121 (2003).
[20] P. Ravindran, A. Kjekshus, H. Fjellvåg, A. Delin, and O. Eriksson, Phys. Rev. B **65**, 064445 (2002).
[21] T. Nakajima, H. Yoshizawa, and Y. Ueda, J. Phys. Soc. Jpn. **73**, 2283 (2004).
[22] R. Vidya, P. Ravindran, H. Fjellvåg, and A. Kjekshus, Phys. Rev. B **74**, 054422 (2006).
[23] R. Vidya, P. Ravindran, K. Knizek, A. Kjekshus, and H. Fjellvåg (unpublished).